Communication

Surface-Enhanced Raman Spectroscopy to Probe Photoreaction Pathways and Kinetics of Isolated Reactants on Surfaces: Flat vs. Curved Substrates

Yue Bing Zheng, John L. Payton, Tze-Bin Song, Bala Krishna Pathem, Yuxi Zhao, Hong Ma, Yang Yang, Lasse Jensen, Alex K. -Y. Jen, and Paul S. Weiss

Nano Lett., **Just Accepted Manuscript** • Publication Date (Web): 14 Sep 2012

Surface-Enhanced Raman Spectroscopy to Probe Photoreaction Pathways and Kinetics of Isolated Reactants on Surfaces: Flat vs. Curved Substrates

Yue Bing Zheng,[1,2,3] John L. Payton,[4] Tze-Bin Song,[1,3] Bala Krishna Pathem,[1,2,3] Yuxi Zhao,[1,2] Hong Ma,[5] Yang Yang,[1,3,*] Lasse Jensen,[4,*] Alex K.-Y. Jen,[5,*] and Paul S. Weiss[1,2,3,4,*]

[1]*California NanoSystems Institute, University of California, Los Angeles, Los Angeles, California 90095, United States*

[2]*Department of Chemistry & Biochemistry, University of California, Los Angeles, Los Angeles, California 90095, United States*

[3]*Department of Materials Science & Engineering, University of California, Los Angeles, Los Angeles, California 90095, United States*

[4]*Department of Chemistry, The Pennsylvania State University, University Park, Pennsylvania 16802, United States*

[5]*Department of Materials Science and Engineering, University of Washington, Seattle, Washington 98195, United States*

[*]To whom correspondence should be addressed: yangy@ucla.edu (Y.Y.); jensen@chem.psu.edu (L.J.); ajen@u.washington.edu (A.K.-Y.J.); psw@cnsi.ucla.edu (P.S.W.)

ABSTRACT

We identify and control the photoreaction paths of self-assembled monolayers (SAMs) of thiolate-linked anthracene phenylethynyl molecules on Au substrate surfaces, and study the effects of nanoscale morphology of substrates on regioselective photoreactions. Two types of morphologies – atomically flat and curved – are produced on Au surfaces by controlling substrate structure and metal deposition. We employ surface-enhanced Raman spectroscopy (SERS), combined with Raman mode analyses using density functional theory, to identify the different photoreaction paths and to track the photoreaction kinetics and efficiencies of molecules in monolayers. The SAMs on curved surfaces exhibit dramatically lower regioselective photoreaction kinetics and efficiencies than those on atomically flat surfaces. This result is attributed to the increased intermolecular distances and variable orientations on the curved surfaces. Better understanding of the morphological effects of substrates will enable control of nanoparticle functionalization in ligand exchange, in targeted delivery of therapeutics and theranostics, and in catalysis.

Keywords: photoreaction, regioselectivity, surface-enhanced Raman spectroscopy, self-assembled monolayers, nansocale morphology, density functional theory

Self-assembled monolayers (SAMs) of molecules are easily prepared on substrates of all sizes and morphologies. They serve as critical components for stabilizing pre-prepared nanostructures with added function or as major functional components, linking molecular-level structures to macroscopic phenomena such as bending, rotation, and wetting.[1-7] Photoreactions within SAMs are one of the most important phenomena that underpin such applications as molecular-scale photolithography and nanoscale optoelectronics.[8-11] With the ever-shrinking size features of functional structures and devices, molecular-level control of adsorption is becoming increasingly important.[8] Precise control makes the surface morphology of substrates one of the major factors that influence adsorption and photoreaction kinetics and efficiencies since most surfaces in practical applications deviate from ideal atomic flatness.[12-14] Likewise, nanoscale catalysts have facets, edges, vertices, and curvatures that influence their efficiencies.[15-17] Ligand-exchange reactions and insertion of functional molecules are critical to creating targeted drug delivery vehicles and theranostic nanoparticles.[18-27] A number of groups have explored using bulky ligands to fill the volume around nanoparticles so as to limit access to the substrate core.[28-37]

Depending on the preparation process and specific substrates, Au surfaces, which are frequently used for SAMs, exhibit a range of morphologies. Ideally, single crystals or epitaxial Au{111} on mica provide atomically flat terraces for scanning tunneling microscopy (STM) imaging of photoreactions at the single-molecule level.[38-48] Au films made by electron-beam deposition or sputtering have surfaces with uncertain orientation and significant roughness. Au nanoparticles synthesized chemically have faceted, flat, or curved surfaces.[12,49,50] To study the reactions of SAMs on these heterogeneous Au surfaces, ensemble techniques, including infrared spectroscopy, X-ray photoelectron spectroscopy, and contact angle measurements, are used.[51] Different characterization techniques with varying substrate surfaces make it challenging to

compare reactions for insight into the effects of substrate morphology. Here, we detail our experimental strategies based on surface-enhanced Raman spectroscopy (SERS) to investigate the photoreaction paths of 9-(4-mercapto-phenylethynyl)anthracene (MPEA) SAMs and the effects of substrate morphology on the photoreaction. Anthracene is an important candidate functionality for organic electronics, optoelectronics, and surface photochemistry.[52,53] In solution, [4+2] photocycloaddition of 9-phenylethynylanthracene (PEA) is favored.[54] Our previous measurements of isolated MPEA pairs held in an inert SAM matrix revealed that the [4+4] regioselective photoreaction occurs when the molecules are restrained by their surroundings.[8] Herein, we aim to identify the photoreaction paths for SAMs of MPEA by recording the fingerprints of reactants and products with SERS. Further, as illustrated in Fig. 1a, we measure and compare the photoreaction kinetics and efficiencies of the SAMs of MPEA on atomically flat *vs.* curved surfaces as a probe of the relative orientations of proximate pairs of adsorbed molecules. The physical mechanism behind the observed differences in the photoreactions on these two types of substrates is described.

We apply SERS to study the photoreaction on both atomically flat and curved surfaces due to its: applicability to substrates regardless of morphology, non-invasiveness, single-molecule sensitivity, and fingerprint signatures.[55-61] To work as SERS substrates, cylindrical nanoholes in square arrays were fabricated into atomically flat expitaxial Au thin films on mica with focused ion beam (FIB) lithography (Nova 600 NanoLab, FEI Company, Hillsboro, OR, USA). The nanoholes have a diameter of 175 nm; the array period is varied within a range from 280 to 450 nm to tune the plasmon resonances to the excitation laser wavelength for maximizing the enhancement of Raman signals.[56] Figure 1b shows a representative scanning electron microscopy (SEM) image of a nanohole array with a hole diameter of 175 nm and a period of 300 nm. The

substrates with nanoscale curved surfaces are the Klarite SERS detection substrates from Renishaw Diagnostics. The substrates themselves consist of a silicon surface, systematically designed with an inverse pyramid pattern, which is then coated with gold. The gold layers consist of particles that have nanoscale curvature (fig. 1c). Both substrates were incubated in 0.1 mM ethanolic solution of MPEA for 24 h. The MPEA was synthesized as described previously.[62] The Au/Mica substrates were annealed with a hydrogen flame immediately prior to incubation. The Klarite substrates were used as purchased. The structures of the SAMs on atomically flat Au surfaces were studied by STM.[8,62,63]

In order to apply SERS to monitor the photoreaction kinetics on surfaces, we start by developing strategies for SERS identification of [4+2] and [4+4] photocycloaddition of 9-phenylethynylanthracene (PEA).[8] We perform density functional theory (DFT) calculations of the Raman spectra of PEA, the thiol(ate) form of which was used in the experiments, and the photoproducts in solution and the SAMs, respectively (fig. 2a). We have examined the dependence of the spectrum on the mole fractions of the products. All calculations were done using the NWChem program package.[64] The B3LYP hybrid functional with the 6-31G* basis set were employed for all calculations of the geometric structure, vibrational frequencies, and Raman differential cross-section.[65] To correct for anharmonicity, vibrational frequencies were scaled by 0.9614; no imaginary frequencies were found. The Raman differential cross sections were calculated by a three-point numerical differentiation of the analytical static polarizability tensors. The cross sections were broadened by a Lorentzian with full-width-at-half-maximum of 20 cm^{-1}.[66]

Figure 2b shows the simulated Raman spectra for PEA, the [4+2] product, and the [4+4] product. The simulated Raman spectra of the various mole fractions of the reactant and product spectra are also presented for the [4+2] (fig. 2c) and [4+4] (fig. 2d) photoreactions. To track the photoreaction of SAMs experimentally, we recorded a series of SERS spectra while samples were exposed to UV (365 nm) light. Raman analyses were performed in a backscattering geometry in a confocal configuration at room temperature with polarized light using a Renishaw inVia Raman system (Renishaw, Inc., Chicago, Illinois, USA). A 632.8 nm He–Ne laser was used as the Raman excitation source; the laser power and beam diameter were 17 mW and 1 μm, respectively. The time-dependent spectra upon irradiation of UV light are shown in fig. 3a (atomically flat surfaces) and fig. 3b (curved surfaces), respectively. The duration (in minutes) of the light irradiation is indicated near the corresponding Raman spectra. The simulated and experimental spectra for PEA (i.e., R:P = 2:0 in fig 2 and at time zero in fig. 3, respectively) are in good agreement. For both spectra, we observe that the photoproducts' Raman intensities are nearly an order of magnitude weaker than the PEA reactant. This is in agreement with the notion that less conjugated systems are weaker Raman scatterers. The experimental spectra exhibit a similar intensity reduction as the photoreaction proceeds.

To address the question of which photoreaction is occurring in experimental measurements on the metal surface, we examined the six major peaks from 1300-1700 cm^{-1}. The experimental and simulated spectra are in excellent agreement as to the positions and relative intensities for these modes. The five major modes from 1300-1550 cm^{-1} are generally in-plane anthracene breathing modes of PEA while the sixth mode at 1594 cm^{-1} is predominantly an in-plane phenyl breathing mode. As seen in Fig. 2d, these anthracene modes are all practically eliminated as the [4+4] photoreaction proceeds, which is understandable because the [4+4] photoproduct no longer has

any anthracene rings. However, it is important to note that PEA's anthracene modes are *not* eliminated, but are rather significantly shifted by a few hundred cm^{-1} because of the loss of the double bonds in the [4+4] photoreaction.

The [4+2] photoproduct, however, does retain one anthracene ring, and in fig. 2c, we observe that the anthracene modes survive the photoreaction, albeit with reduced intensities. However, the intensity of the anthracene ring mode at 1399 cm^{-1} in the [4+2] photoreaction is nearly unaffected by the photoreaction, whereas in the [4+4] photoreaction this mode does not exist for the photoproduct. This result provides us with a tool to determine whether the experimental photoreaction pathway is [4+4] or [4+2]. In fig. 3 (the experimental spectra), we observe this mode being eliminated by the photoreaction, an indication that the experimental reaction on the surface proceeds via a [4+4] mechanism. In order to have a clearer picture of the photoreaction, we studied the ratios of the peak areas of the 1399 cm^{-1} anthracene ring mode (indicated as P2 in figs. 2 and 3) and the peak area of the 1594 cm^{-1} phenyl mode of the tether (indicated as P3 in figs. 2 and 3). Figure 4 shows the modes. In fig. 5a, we present the peak area ratio P2/P3 as a function of the fraction of product for the simulated spectra in Fig. 2. In fig. 5b,c, we present P2/P3 as a function of UV irradiation time for the experimental spectra in fig. 3. The error bars are determined by the standard deviations of the peak area ratios in four sets of measurements. We chose the phenyl mode as an internal standard because it is relatively unaffected by the photoreaction as to its displacement vectors and Raman intensity. From fig. 5a, we can see that there is a qualitative difference between the two photoreactions. The ratio for the [4+4] reaction decreases as reactants are converted into products, opposite to the trend predicted for the [4+2] reaction. The experimental peak area ratios decrease as the photoreaction proceeds, consistent

with the [4+4] reaction. This indicates that the experimental reaction is indeed a [4+4] photoreaction.

To track the photoreaction kinetics of the SAMs, we choose the P1 mode as identified in figs. 2 and 3 (see fig. 4 for the mode) because it has relatively strong signals in the experimental spectra, which are subject to change as the photoreaction proceeds. We calculate the ratios between the peak areas of modes P1 and P3 for each experimental spectrum in fig. 3. A plot of P1/P3 as a function of UV irradiation time is plotted as P1/P3 vs. time (fig. 6). The error bars are determined by the standard deviations of the peak area ratios from four sets of measurements. As shown in figs. 6a and b, both samples exhibit monotonic trends as a function of UV light exposure time. Detailed comparisons of the figs. 6a and 6b show that the peak area ratios P1/P2 decreased much more rapidly for the SAMs on atomically flat surfaces; while P1/P2 reached 0 (indicating complete photoreaction) after ~7 h of UV exposure (~573 $\mu W/cm^2$, 365 nm) for the SAMs on atomically flat surfaces, P1/P2 for the curved surfaces did not reach 0 even after UV exposure for 16 h. We infer that the slower reaction kinetics and lower efficiency of the SAMs on the curved surfaces arise from the larger intermolecular distances and variable orientations in the SAMs (Fig. 1a).

To gain insight into the molecular orientations (as illustrated in schematics of Fig. 1a) on curved and planar surfaces, we compare the SERS spectra of the as-prepared SAMs (before UV irradiation) of MPEA in figs. 3a and 3b. Density functional theory calculations of PEA pairs as a function of tilt angle θ (as defined in fig. 7) are used for reference. Figure 7 shows two configurations of a PEA pair: (fig. 7a) parallel PEA molecules with inter-planar distances of 3.2 Å in a face-to-face orientation (θ =0°) and (fig. 7b) PEA molecules tilted 15° (θ =15°, so

the molecule-molecule angles are 30°). Figure 7c shows the B3LYP/6-31G* Raman spectra of PEA pair computed as function of tilt angle θ. We observe an increase in intensity as the angle changes from θ = 0° to 15°, due to decreased intermolecular interactions in the tilted PEA pair. This effect of tilt angle on the Raman intensity is consistent with our previous study.[67] The more interesting data is the ratio of peaks at 1545 and 1594 cm^{-1}. The 1545 cm^{-1} mode is an anthracene mode and 1594 cm^{-1} is a phenyl ring mode. We indicate the peak areas of 1545 and 1594 cm^{-1} by P1545 and P1594, respectively. As a result, at θ =0°, P1545/P1594 = 0.95 and, at θ = 15°, P1545/P1594 = 1.1, indicating that the increased tilt angle corresponds to an increased ratio (P1545/P1594). From the experimental spectra in Figs. 3a and 3b, we obtain the peak area ratios for planar and curved surfaces are 0.2 and 0.48, respectively. The increased peak area ratio for the curved surface reveals that molecules on the curved surfaces tend to be tilted from each other. We propose that such molecules (molecular pairs) can be used to probe the local chemical environment on curved surfaces vis-à-vis ligand-exchange reactions,[29-31,68,69] surface reactions,[28,70,71] bioavailability of chemical functionality for targeted delivery and selective capture.[19-25,33-37,72] We are now pursuing this line of research by developing other molecules to probe this important interface.

In summary, we have shown that SERS is capable of probing the photoreaction paths of molecules in SAMs and the effects of nanoscale morphology of substrates on the photoreaction kinetics. Incorporation of nano- and/or micro-scale features into the substrates enables us to monitor the reactions of SAMs with SERS, which has high sensitivity in identifying and monitoring the fingerprints of the reactants and products.[56,73] The interpretation of the experimental SERS data is critically supported by DFT calculations. We observe slower kinetics and lower efficiency for reactions on curved surfaces, and attribute this to the larger

intermolecular distances and variable molecular orientations on curved vs. flat surfaces, confirmed spectroscopically. Our study reveals the critical role of substrate morphology in determining photochemistry and photophysics of photoactive adsorbates, suggesting opportunities for nanoscale surface engineering for controlling reactions and furthering applications of surface chemistry and nanoparticle functionalization.

Acknowledgments

We thank the Department of Energy (Grant #DE-FG02-07ER15877) and the Kavli Foundation for support of the work described here. B. K. P. thanks the Penn State Center for Nanoscale Science (a NSF-supported Materials Research Science and Engineering Center) for support. The Raman simulations were supported through the CAREER program of the NSF (Grant #CHE-0955689). The substrates were fabricated at the California NanoSystems Institute. We thank Noah Bodzin at UCLA for assistance with focused ion beam lithography.

References

1. Hohman, J. N.; Kim, M.; Wadsworth, G. A.; Bednar, H. R.; Jiang, J.; LeThai, M. A.; Weiss, P. S. *Nano Lett.* **2011,** *11*, 5104-5110.

2. Davis, J. J.; Orlowski, G. A.; Rahman, H.; Beer, P. D. *Chem. Commun.* **2010,** *46*, 54-63.

3. Huang, T. J.; Brough, B.; Ho, C. M.; Liu, Y.; Flood, A. H.; Bonvallet, P. A.; Tseng, H. R.; Stoddart, J. F.; Baller, M.; Magonov, S. *Appl. Phys. Lett.* **2004,** *85*, 5391-5393.

4. Juluri, B. K.; Kumar, A. S.; Liu, Y.; Ye, T.; Yang, Y. W.; Flood, A. H.; Fang, L.; Stoddart, J. F.; Weiss, P. S.; Huang, T. J. *ACS Nano* **2009,** *3*, 291-300.

5. Li, D. B.; Paxton, W. F.; Baughman, R. H.; Huang, T. J.; Stoddart, J. F.; Weiss, P. S. *MRS Bull.* **2009,** *34*, 671-681.

6. Michl, J.; Sykes, E. C. H. *ACS Nano* **2009,** *3*, 1042-1048.

7. Berna, J.; Leigh, D. A.; Lubomska, M.; Mendoza, S. M.; Perez, E. M.; Rudolf, P.; Teobaldi, G.; Zerbetto, F. *Nature Mater.* **2005,** *4*, 704-710.

8. Kim, M.; Hohman, J. N.; Cao, Y.; Houk, K. N.; Ma, H.; Jen, A. K. Y.; Weiss, P. S. *Science* **2011,** *331*, 1312-1315.

9. Saavedra, H. M.; Mullen, T. J.; Zhang, P. P.; Dewey, D. C.; Claridge, S. A.; Weiss, P. S. *Rep. Prog. Phys.* **2010,** *73*, 036501.

10. Smith, R. K.; Lewis, P. A.; Weiss, P. S. *Prog. Surf. Sci.* **2004,** *75*, 1-68.

11. Zheng, Y. B.; Pathem, B. K.; Hohman, J. N.; Thomas, J. C.; Kim, M.; Weiss, P. S. *Adv. Mater*. **2012**, *24*, in press. DOI: 10.1002/adma.201201532.

12. Hill, H. D.; Millstone, J. E.; Banholzer, M. J.; Mirkin, C. A. *ACS Nano* **2009,** *3*, 418-424.

13. Cederquist, K. B.; Keating, C. D. *Langmuir* **2010,** *26*, 18273-18280.

14. Suda, M.; Kameyama, N.; Suzuki, M.; Kawamura, N.; Einaga, Y. *Angew. Chem. Int. Ed.* **2008,** *47*, 160-163.

15. Boucher, M. B.; Goergen, S.; Yi, N.; Flytzani-Stephanopoulos, M. *Phys. Chem. Chem. Phys.* **2011,** *13*, 2517-2527.

16. Huang, X.-S.; Sun, H.; Wang, L.-C.; Liu, Y.-M.; Fan, K.-N.; Cao, Y. *Appl. Catal. B-Environ.* **2009,** *90*, 224-232.

17. Liu, L.; Yao, Z.; Deng, Y.; Gao, F.; Liu, B.; Dong, L. *ChemCatChem* **2011,** *3*, 978-989.

18. Xu, X.; Rosi, N. L.; Wang, Y.; Huo, F.; Mirkin, C. A. *J. Am. Chem. Soc.* **2006,** *128*, 9286-9287.

19. Bertin, P. A.; Gibbs, J. M.; Shen, C. K.-F.; Thaxton, C. S.; Russin, W. A.; Mirkin, C. A.; Nguyen, S. T. *J. Am. Chem. Soc.* **2006,** *128*, 4168-4169.

20. Farokhzad, O. C.; Langer, R. *ACS Nano* **2009,** *3*, 16-20.

21. Prigodich, A. E.; Seferos, D. S.; Massich, M. D.; Giljohann, D. A.; Lane, B. C.; Mirkin, C. A. *ACS Nano* **2009,** *3*, 2147-2152.

22. Barth, B. M.; Sharma, R.; Altınoğlu, E. I.; Morgan, T. T.; Shanmugavelandy, S. S.; Kaiser, J. M.; McGovern, C.; Matters, G. L.; Smith, J. P.; Kester, M.; Adair, J. H. *ACS Nano* **2010,** *4*, 1279-1287.

23. Moghimi, S. M.; Peer, D.; Langer, R. *ACS Nano* **2011,** *5*, 8454-8458.

24. Gianella, A.; Jarzyna, P. A.; Mani, V.; Ramachandran, S.; Calcagno, C.; Tang, J.; Kann, B.; Dijk, W. J. R.; Thijssen, V. L.; Griffioen, A. W.; Storm, G.; Fayad, Z. A.; Mulder, W. J. M. *ACS Nano* **2011,** *5*, 4422-4433.

25. Xiao, Z.; Levy-Nissenbaum, E.; Alexis, F.; Lupták, A.; Teply, B. A.; Chan, J. M.; Shi, J.; Digga, E.; Cheng, J.; Langer, R.; Farokhzad, O. C. *ACS Nano* **2012,** *6*, 696-704.

26. Klajn, R.; Stoddart, J. F.; Grzybowski, B. A. *Chem. Soc. Rev.* **2010,** *39*, 2203-2237.

27. Klajn, R. *Pure Appl. Chem.* **2010,** *82*, 2247-2279.

28. Templeton, A. C.; Hostetler, M. J.; Kraft, C. T.; Murray, R. W. *J. Am. Chem. Soc.* **1998,** *120*, 1906-1911.

29. Weeraman, C.; Yatawara, A. K.; Bordenyuk, A. N.; Benderskii, A. V. *J. Am. Chem. Soc.* **2006,** *128*, 14244-14245.

30. Mei, B. C.; Oh, E.; Susumu, K.; Farrell, D.; Mountziaris, T. J.; Mattoussi, H. *Langmuir* **2009,** *25*, 10604-10611.

31. Jones, R. L.; Pearsall, N. C.; Batteas, J. D. *J. Phys. Chem. C* **2009,** *113*, 4507-4514.

32. Hohman, J. N.; Claridge, S. A.; Kim, M.; Weiss, P. S. *Mat. Sci. Eng. R* **2010,** *70*, 188-208.

33. Krommenhoek, P. J.; Wang, J.; Hentz, N.; Johnston-Peck, A. C.; Kozek, K. A.; Kalyuzhny, G.; Tracy, J. B. *ACS Nano* **2012,** *6*, 4903-4911.

34. Cutler, J. I.; Auyeung, E.; Mirkin, C. A. *J. Am. Chem. Soc.* **2012,** *134*, 1376-1391.

35. Zheng, D.; Giljohann, D. A.; Chen, D. L.; Massich, M. D.; Wang, X.-Q.; Iordanov, H.; Mirkin, C. A.; Paller, A. S. *Proc. Natl. Acad. Sci. USA* **2012,** in press. DOI: 10.1073/pnas.1118425109.

36. Albanese, A.; Tang, P. S.; Chan, W. C. W. *Annu. Rev. Biomed. Eng.* **2012,** *14*, 1-16.

37. Pelaz, B.; Jaber, S.; Jimenez de Aberasturi, D.; Wulf, V.; Aida, T.; de la Fuente, J. M.; Feldmann, J.; Gaub, H. E.; Josephson, L.; Kagan, C. R.; Kotov, N. A.; Liz-Marzán, L. M.; Mattoussi, H.; Mulvaney, P.; Murray, C. B.; Rogach, A. L.; Weiss, P. S.; Willner, I.; Parak, W. J. *ACS Nano* **2012**, *6*, in press. DOI: 10.1021/nn303929a.

38. Donhauser, Z. J.; Mantooth, B. A.; Kelly, K. F.; Bumm, L. A.; Monnell, J. D.; Stapleton, J. J.; Price, D. W.; Rawlett, A. M.; Allara, D. L.; Tour, J. M.; Weiss, P. S. *Science* **2001,** *292*, 2303-2307.

39. Bumm, L. A.; Arnold, J. J.; Cygan, M. T.; Dunbar, T. D.; Burgin, T. P.; Jones, L.; Allara, D. L.; Tour, J. M.; Weiss, P. S. *Science* **1996,** *271*, 1705-1707.

40. Comstock, M. J.; Levy, N.; Kirakosian, A.; Cho, J. W.; Lauterwasser, F.; Harvey, J. H.; Strubbe, D. A.; Frechet, J. M. J.; Trauner, D.; Louie, S. G.; Crommie, M. F. *Phys. Rev. Lett.* **2007,** *99*, 038301.

41. van der Molen, S. J.; van der Vegte, H.; Kudernac, T.; Amin, I.; Feringa, B. L.; van Wees, B. J. *Nanotechnology* **2006,** *17*, 310-314.

42. Kumar, A. S.; Ye, T.; Takami, T.; Yu, B. C.; Flatt, A. K.; Tour, J. M.; Weiss, P. S. *Nano Lett.* **2008,** *8*, 1644-1648.

43. Lewis, P. A.; Inman, C. E.; Yao, Y. X.; Tour, J. M.; Hutchison, J. E.; Weiss, P. S. *J. Am. Chem. Soc.* **2004,** *126*, 12214-12215.

44. Lewis, P. A.; Inman, C. E.; Maya, F.; Tour, J. M.; Hutchison, J. E.; Weiss, P. S. *J. Am. Chem. Soc.* **2005,** *127*, 17421-17426.

45. Donhauser, Z. J.; Price, D. W.; Tour, J. M.; Weiss, P. S. *J. Am. Chem. Soc.* **2003,** *125*, 11462-11463.

46. Cygan, M. T.; Dunbar, T. D.; Arnold, J. J.; Bumm, L. A.; Shedlock, N. F.; Burgin, T. P.; Jones, L.; Allara, D. L.; Tour, J. M.; Weiss, P. S. *J. Am. Chem. Soc.* **1998,** *120*, 2721-2732.

47. Bumm, L. A.; Arnold, J. J.; Charles, L. F.; Dunbar, T. D.; Allara, D. L.; Weiss, P. S. *J. Am. Chem. Soc.* **1999,** *121*, 8017-8021.

48. Claridge, S. A.; Schwartz, J. J.; Weiss, P. S. *ACS Nano* **2011,** *5*, 693-729.

49. Dahanayaka, D. H.; Wang, J. X.; Hossain, S.; Bumm, L. A. *J. Am. Chem. Soc.* **2006,** *128*, 6052-6053.

50. Xue, C.; Métraux, G. S.; Millstone, J. E.; Mirkin, C. A. *J. Am. Chem. Soc.* **2008,** *130*, 8337-8344.

51. Fox, M. A.; Wooten, M. D. *Langmuir* **1997,** *13*, 7099-7105.

52. Anthony, J. E. *Chem. Rev.* **2006,** *106*, 5028-5048.

53. Bouas-Laurent, H.; Castellan, A.; Desvergne, J.-P.; Lapouyade, R. *Chem. Soc. Rev.* **2000,** *29*, 43-55.

54. Becker, H.-D.; Andersson, K. *J. Photochem.* **1984,** *26*, 75-77.

55. Kneipp, K.; Wang, Y.; Kneipp, H.; Perelman, L. T.; Itzkan, I.; Dasari, R.; Feld, M. S. *Phys. Rev. Lett.* **1997,** *78*, 1667-1670.

56. Zheng, Y. B.; Payton, J. L.; Chung, C. H.; Liu, R.; Cheunkar, S.; Pathem, B. K.; Yang, Y.; Jensen, L.; Weiss, P. S. *Nano Lett.* **2011,** *11*, 3447-3452.

57. Ward, D. R.; Halas, N. J.; Ciszek, J. W.; Tour, J. M.; Wu, Y.; Nordlander, P.; Natelson, D. *Nano Lett.* **2008,** *8*, 919-924.

58. Stiles, P. L.; Dieringer, J. A.; Shah, N. C.; Van Duyne, R. R. *Annu. Rev. Anal. Chem.* **2008,** *1*, 601-626.

59. Barhoumi, A.; Halas, N. J. *J. Phys. Chem. Lett.* **2011,** *2*, 3118-3123.

60. Pierre, M. C. S.; Mackie, P. M.; Roca, M.; Haes, A. J. *J. Phys. Chem. C* **2011,** *115*, 18511-18517.

61. Bantz, K. C.; Meyer, A. F.; Wittenberg, N. J.; Im, H.; Kurtulus, O.; Lee, S. H.; Lindquist, N. C.; Oh, S.-H.; Haynes, C. L. *Phys. Chem. Chem. Phys.* **2011,** *13*, 11551-11567.

62. Dou, R.-F.; Ma, X.-C.; Xi, L.; Yip, H. L.; Wong, K. Y.; Lau, W. M.; Jia, J.-F.; Xue, Q.-K.; Yang, W.-S.; Ma, H.; Jen, A. K. Y. *Langmuir* **2006,** *22*, 3049-3056.

63. Zareie, M. H.; Ma, H.; Reed, B. W.; Jen, A. K. Y.; Sarikaya, M. *Nano Lett.* **2003,** *3*, 139-142.

64. Valiev, M.; Bylaska, E. J.; Govind, N.; Kowalski, K.; Straatsma, T. P.; Van Dam, H. J. J.; Wang, D.; Nieplocha, J.; Apra, E.; Windus, T. L.; de Jong, W. *Comput. Phys. Commun.* **2010,** *181*, 1477-1489.

65. Becke, A. D. *J. Chem. Phys.* **1993,** *98*, 5648-5652.

66. Merrick, J. P.; Moran, D.; Radom, L. *J. Phys. Chem. A* **2007,** *111*, 11683-11700.

67. Zheng, Y. B.; Pathem, B. K.; Payton, J. L.; Bob, B.; Kumar, A. S.; Chung, C. H.; Corley, D. A.; Yang, Y.; Jensen, L.; Tour, J. M.; Weiss, P. S. **2012**, in preparation.

68. Puzder, A.; Williamson, A. J.; Zaitseva, N.; Galli, G.; Manna, L.; Alivisatos, A. P. *Nano Lett.* **2004,** *4*, 2361-2365.

69. Owen, J. S.; Park, J.; Trudeau, P.-E.; Alivisatos, A. P. *J. Am. Chem. Soc.* **2008,** *130*, 12279-12281.

70. Schmelmer, U.; Jordan, R.; Geyer, W.; Eck, W.; Gölzhäuser, A.; Grunze, M.; Ulman, A. *Angew. Chem. Int. Ed.* **2003,** *42*, 559-563.

71. Turchanin, A.; El-Desawy, M.; Golzhauser, A. *Appl. Phys. Lett.* **2007,** *90*, 053102.

72. Vaish, A.; Shuster, M. J.; Cheunkar, S.; Singh, Y. S.; Weiss, P. S.; Andrews, A. M. *ACS Chem. Neurosci.* **2010,** *1*, 495-504.

73. Pathem, B. K.; Zheng, Y. B.; Payton, J. L.; Song, T.-B.; Yu, B.-C.; Tour, J. M.; Yang, Y.; Jensen, L.; Weiss, P. S. *J. Phys. Chem. Lett.* **2012**, *3*, 2388-2394.

Figure 1

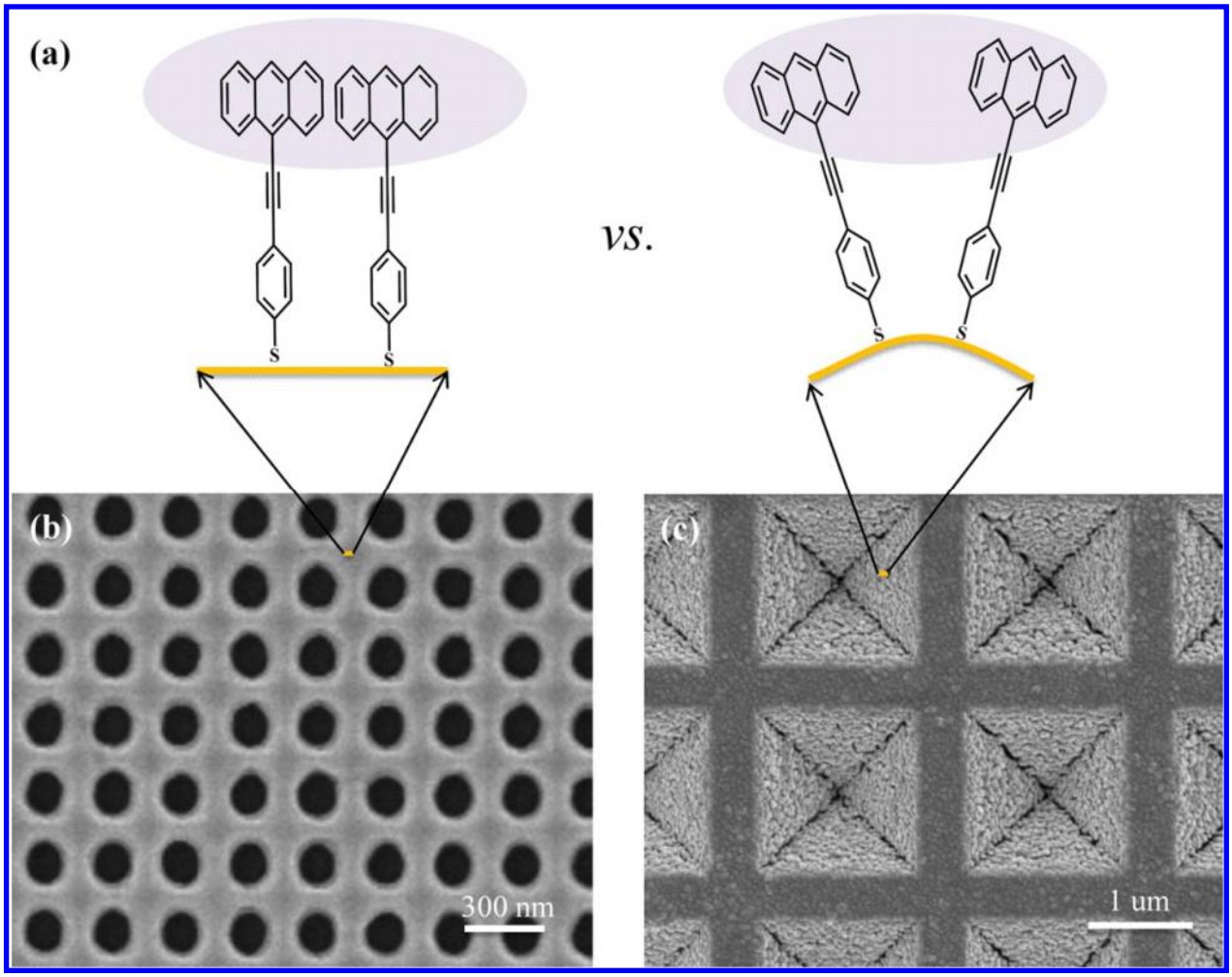

Figure 1: (a) Cross-sectional schematic view of UV-exposed self-assembled monolayers (SAMs) of 9-(4-mercapto-phenylethynyl)anthracene (MPEA) on (left) atomically flat and (right) curved surfaces, respectively. We measure and compare the photoreaction efficiency of these two types of SAMs. (b & c) scanning electron microscopy (SEM) images of the two types of surface-enhanced Raman spectroscopy (SERS) substrates used in the experiments: epitaxial Au on mica with nanohole arrays (with atomically flat Au terraces) and Au nanoparticles on patterned silicon (with resultant curved Au surfaces), also known as Klarite SERS detection substrates from Renishaw Diagnostics. The arrows indicate the schematic as the zoom-in view of the lines (golden color) on the SEM images.

Figure 2

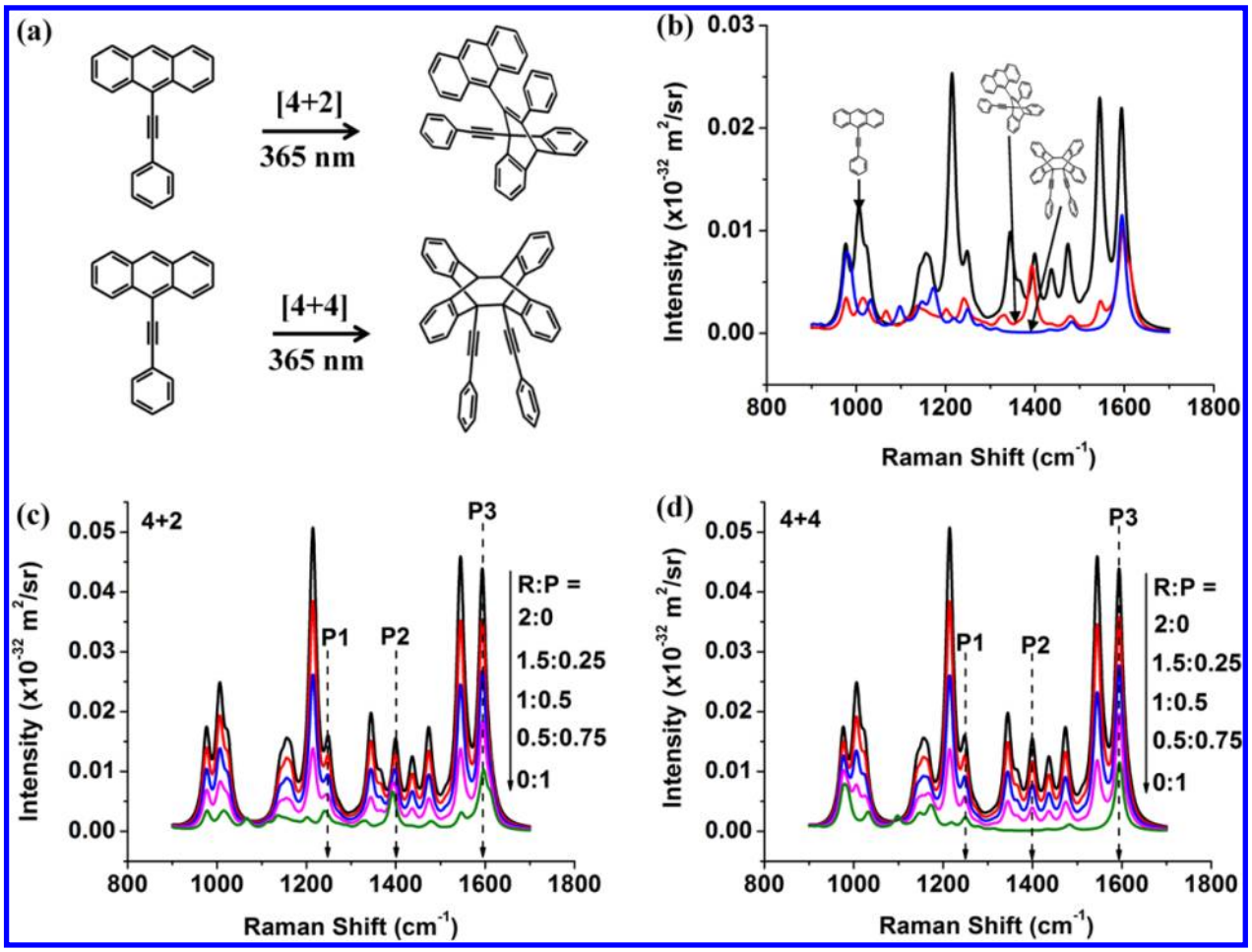

Figure 2: (a) Schematic view of the [4+2] and [4+4] photoreactions of 9-phenylethynylanthracene (PEA). (b) Simulated (B3LYP/6-31G*) Raman spectra of reactant (R), [4+2] product, and [4+4] product. (c) Simulated (B3LYP/6-31G*) Raman spectra of reactant (R), [4+2] product (P), and the various convoluted mole fractions of the two spectra. (d) Simulated Raman spectra of reactant (R), [4+4] product (P), and the various convoluted mole fractions of the two spectra. P1, P2, and P3 indicate the modes that are used in our analyses of the photoreaction paths and kinetics. The solid arrows with various ratios of reactant and product ("R:P") indicate that the spectra from high to low intensity have increased conversion fraction from reactant to product.

Figure 3

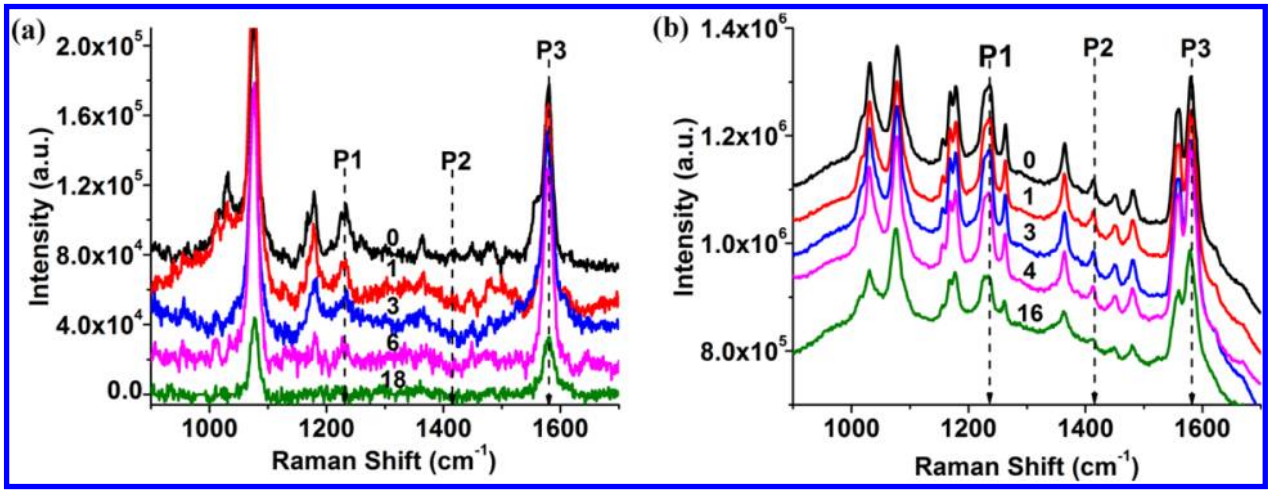

Figure 3: A series of time-dependent SERS spectra after UV (365 nm) exposure of the SAMs of MPEA on (a) atomically flat surfaces and (b) curved surfaces. The exposure time (in hours) is indicated as a number near the corresponding spectra. Vertical offsets of the spectra are used for clarity. In (a), the background signals are subtracted from the original spectra. P1, P2, and P3 indicate the modes that are used in our analyses of the photoreaction paths and kinetics.

Figure 4

Mode / Mode picture / Molecule	P1	P2	P3
PEA	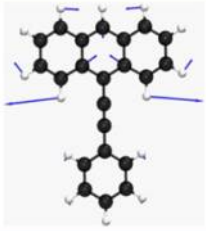	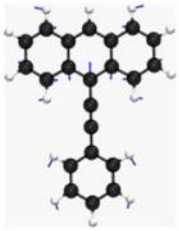	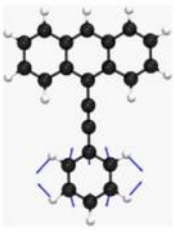
[4+2] product	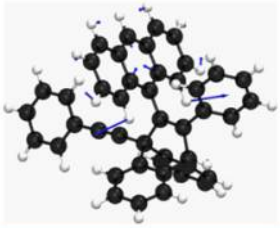	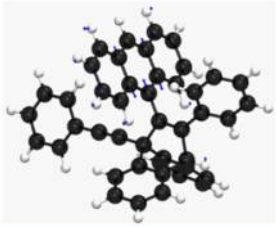	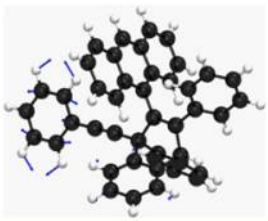
[4+4] product	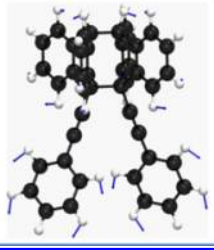	*Do not exist*	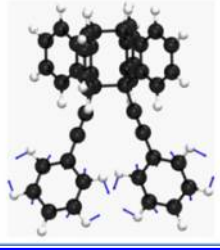

Figure 4: Schematic of P1, P2, and P3 modes for 9-phenylethynylanthracene (PEA), the [4+2] photoreaction product, and the [4+4] photoreaction product.

Figure 5

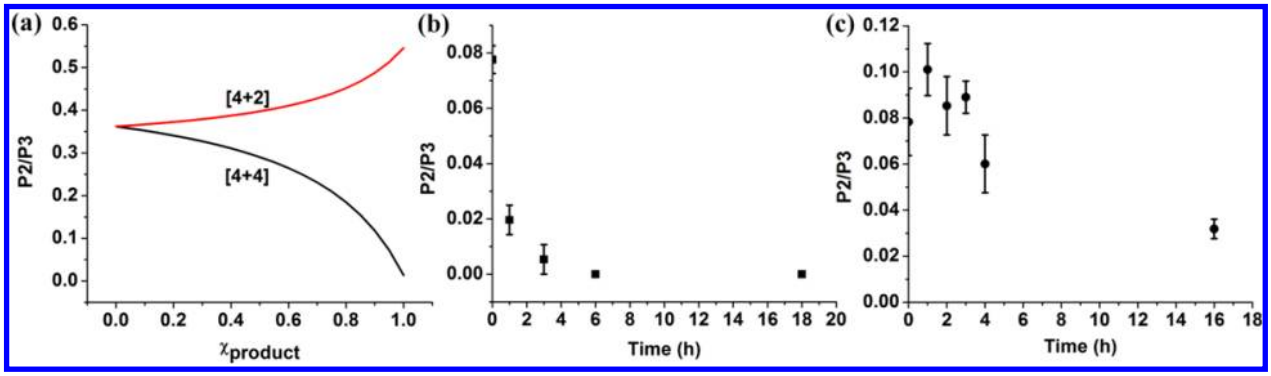

Figure 5: (a) The simulated (B3LYP/6-31G*) peak area ratio (P2/P3) of the Raman modes P2 and P3 as a function of mole fraction ($\chi_{product}$) of the products of [4+2] and [4+4] photoreactions. (b and c) The experimental peak area ratio (P2/P3) of the Raman modes P2 and P3 as a function of UV light exposure time for the SAMs of MPEA on atomically flat surfaces and curved surfaces, respectively.

Figure 6

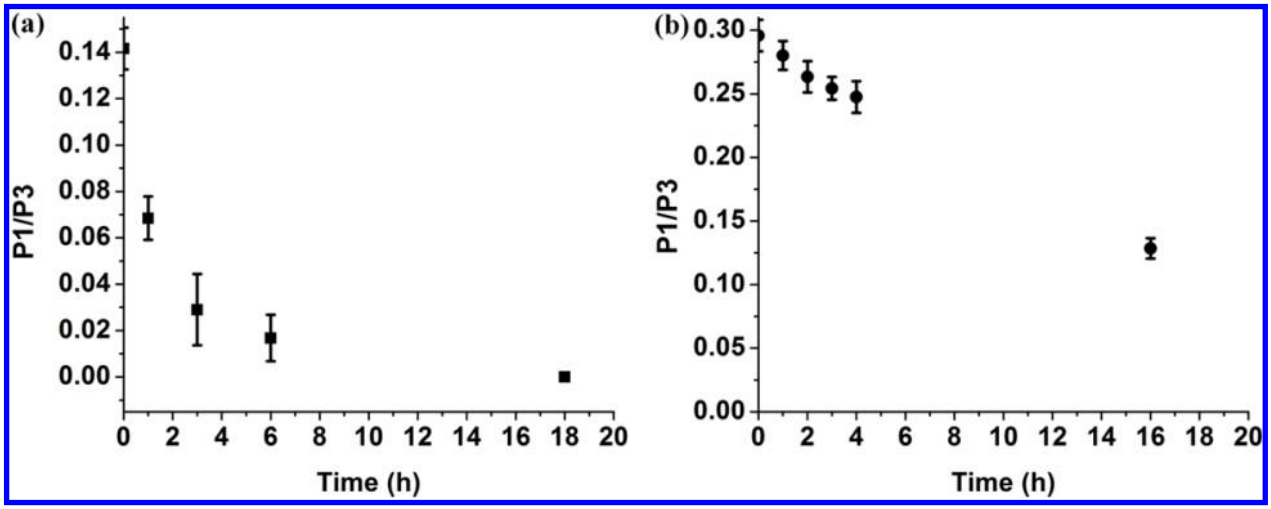

Figure 6: The experimental peak area ratio (P1/P3) of the Raman modes P1 and P3 as a function of UV light exposure time for the SAMs of MPEA on (a) atomically flat surfaces and (b) curved surfaces.

Figure 7

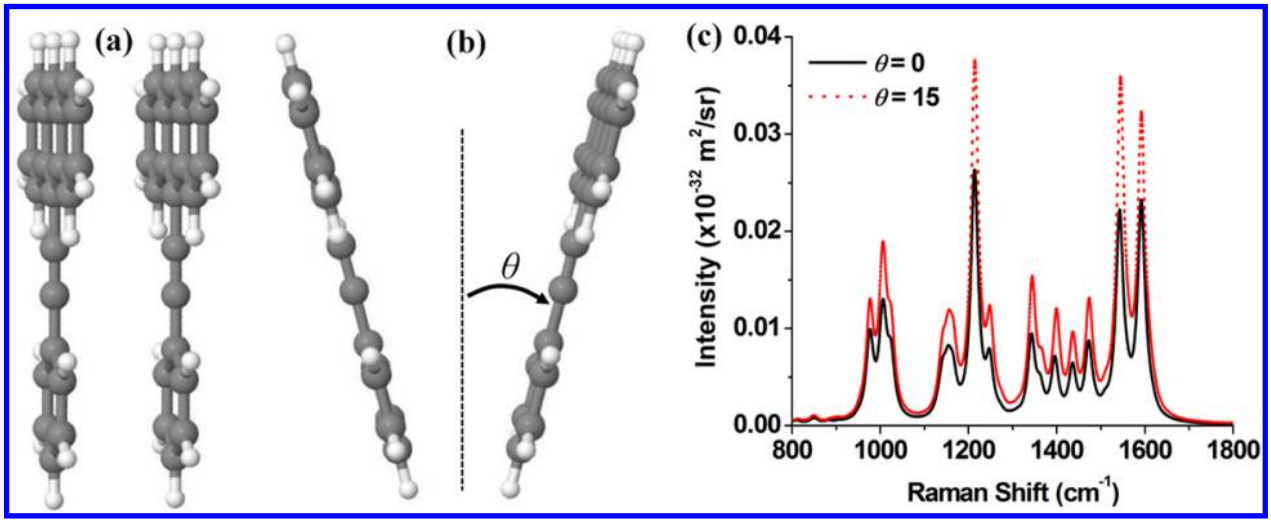

Figure 7: (a) Configuration of a PEA pair parallel to each other with an inter-planar distance of 3.2 Å in a face-to-face orientation. (b) Configuration of a PEA pair tilted away from each other and 15° from the local surface normal (θ =15°). (c) The B3LYP/6-31G* Raman spectra of PEA pairs computed as a function of tilt angle θ. At θ = 0°, the PEA pairs are parallel to each other.

TOC